Photophysical Studies of Formic Acid in the Vacuum UV: Fragmentation, Fluorescence, and Ionization in the 6−23 eV Photon Energy Range†

Martin Schwell,[⊥,‡,§] François Dulieu,[⊥,‡] Hans-Werner Jochims,[#] Jean-Hugues Fillion,[⊥,‡] Jean-Louis Lemaire,[⊥,‡] Helmut Baumgärtel,[#] and Sydney Leach*,[⊥,‡]

DAMAp - UMR 8588, Observatoire de Paris-Meudon, 5 place Jules Janssen, 92195 Meudon, France, LAMAp - UMR 8588, Département de Physique, Université de Cergy-Pontoise, 95031 Cergy Pontoise Cedex, France, and Institut für Physikalische und Theoretische Chemie der Freien Universität Berlin, Takustrasse 3, 14195 Berlin, Germany

Received: March 27, 2002; In Final Form: September 3, 2002

Vacuum-UV (VUV) photodissociation of gaseous formic acid (HCOOH) has been studied in the 6−23 eV range using photofragment fluorescence spectroscopy and synchrotron radiation excitation. Previous studies were limited to the region below 11.4 eV. Emission of OH (A), CH (A, B), HCOO, and H Balmer radiation is observed at various excitation energies in the VUV. Bands in the corresponding fluorescence excitation spectra can be associated with specific absorption bands of HCOOH. The HCOO fluorescence between 330 and 480 nm is assigned to the $^2B_1 \rightarrow {}^2A''$ transition. The quantum yield of photoionization, γ, measured from 10 to 23 eV, reaches unity at 18 ± 0.1 eV. The energy domain, ΔE, of competitive nonionic decay processes of superexcited molecular states above the ionization threshold is thus found to be $\Delta E(\mathrm{HCOOH}) = 6.68 \pm 0.1$ eV. Between 15.7 and 17 eV, Rydberg absorption bands converging to the $3^2A'$ state of $HCOOH^+$ are mirrored in the $\gamma(E_{exc})$ spectrum, from which an autoionization rate $k_{ai} \approx 7.5 \times 10^{13}\ s^{-1}$ was determined for the Rydberg levels. Below the astrophysical HI limit (13.6 eV), the neutral processes HCOOH → OH + HCO and HCOOH → CO_2 + 2H dominate the fragmentation of formic acid. The quantum yield of ionic dissociation processes $HCOOH^+ \rightarrow COOH^+ + H$ and $HCOOH^+ \rightarrow HCO^+ + OH$ is determined to be less than 25% in this energy region. Although the ionic processes become more important between 13.6 and 18 eV, neutral dissociation processes with large quantum yields still occur. The astrophysical relevance of the photophysical properties of formic acid is briefly discussed.

1. Introduction

Absorption of vacuum-UV (VUV) photons by a molecule opens up many photophysical processes, including a variety of relaxation processes.[1] Previous studies of the VUV spectroscopy and photophysics of the astrophysically interesting species formic acid (HCOOH) have been mainly limited to absorption and fluorescence measurements below 11.4 eV,[2−4] apart from a photoionization mass spectrometric study up to 19 eV.[5] This 11.4 eV limit, essentially due to experimental restrictions on window transparency in the VUV, also exists for studies on many other small molecules important in prebiotic chemistry and which are also observed in the interstellar medium (ISM). This can be seen, for example, in the photoabsorption spectra of molecules related to formic acid, such as acetic acid (CH_3-COOH) and its isomer methyl formate ($HCOOCH_3$).[2] We remark that the VUV photoabsorption of these molecules is often much stronger than the UV photoabsorption[2] and that at E = 10.2 eV, at which the intense Lyman-α emission of stars is located, they are found to absorb strongly. We further note that the VUV photon flux from the early sun was probably 10−100 times greater than is the case today, although the total spectral luminosity was less.[6] This gives additional interest to exploration of the VUV photophysics of prebiotic species such as formic acid.

Photodissociation and dissociative photoionization processes[1] can give rise to reactive species such as radicals and ions, which can be formed not only in the ground but also in electronically or vibrationally excited states or both, as will be seen to be the case in formic acid. This species, as well as many other small molecules, is observed in the ISM, so improvement of molecular cloud astrochemical models[7] requires photophysical data both below and above the experimental 11.4 eV limit, in particular because important processes, such as neutral photodissociation, photoionization, and dissociative photoionization, can be very efficient in the VUV. Furthermore, ion−molecule reactions are thought to play an important role in the formation of interstellar molecules in dense clouds.[7]

We have carried out extensive studies on the spectroscopy and photophysics of formic acid in the 6−23 eV energy region. A detailed analysis of the 6−23 eV photoabsorption spectrum has been made,[8] and the He(I) photoelectron spectra of HCOOH and its isotopologues HCOOD, DCOOH, and DCOOD have been recorded and analyzed.[9] In the present work, we have used photofragment fluorescence spectroscopy as an analytical tool to provide insight into the photoprocesses of formic acid (for a recent review of this method, see ref 10 and references therein). We have also measured the quantum yield of ionization of

† Part of the special issue "R. Stephen Berry Festschrift".

* To whom correspondence should be addressed. E-mail: sydney.leach@obspm.fr. Fax: +33-1 4507 7100.

⊥ Observatoire de Paris-Meudon.

‡ Université de Cergy-Pontoise.

§ Present address: Laboratoire Interuniversitaire des Systèmes Atmosphériques (LISA), Université Paris 7 et 12, 61 Avenue du Général de Gaulle, 94010 Creteil Cedex, France.

Institut für Physikalische und Theoretische Chemie der Freien Universität Berlin.

10.1021/jp020809t CCC: $22.00
Published on Web 10/16/2002

HCOOH as a function of photon excitation energy. This is an important parameter in the modeling of astrophysical processes involving formic acid.

Identification of the emission features observed in the dispersed fluorescence spectra of HCOOH is followed by a fluorescence excitation (FEX) spectral study of the excitation energy dependence of these features. Particular attention is paid to the identification and assignment of emission from the HCOO radical. Analysis of the FEX spectra and the ionization quantum yield measurements is made with the aid of data from the VUV absorption spectra and the He(I) photoelectron spectrum. This information is also used to suggest new interpretations of the photoionization breakdown curves of formic acid,[5] as well as to discuss some astrophysical observations involving this species.

2. Experimental Section

Monochromatized synchrotron radiation was obtained from the Berlin electron storage ring BESSY I (multibunch mode) in association with a 1.5 m McPherson monochromator (normal incidence (NIM), dispersion 5.6 Å/mm). Complementary experiments, with the same equipment, were performed at LURE/Orsay (SA63 beamline, 3 m NIM monochromator).

The grating transmission function of the monochromator is recorded by detecting the visible fluorescence emitted by the sodium salicylate layer placed on a quartz window. For fluorescence measurements, the synchrotron light beam is focused into an open brass cell, differentially pumped, containing formic acid vapor at a pressure typically around 10^{-3} mbar. Fluorescence induced in the irradiated target molecules passes through a quartz window and is dispersed using a 20 cm focal length secondary monochromator (Jobin-Yvon H 20 UV, grating blazed at 300 nm). This monochromator has a fixed, exchangeable exit slit but has no entrance slit. The width of the effective "entrance slit" is given by the spatial extension of the exciting light beam (approximately 1 mm). The emitted fluorescence light, measured in the 250−550 nm wavelength range, is detected by a photon-counting Hamamatsu R6060 photomultiplier, cooled to 250 K by a Peltier element. The spectral response function of this arrangement has been determined by recording the spectrum emitted by a tungsten halogen lamp, which is then deconvoluted according to Planck's law. A dispersed fluorescence spectrum typically contains 1 point per 2 nm. The resolution of these spectra is between 5 and 8 nm depending on the choice of the effective exit slit width.

In recording the fluorescence excitation (FEX) spectra, the secondary monochromator is fixed at a desired wavelength with a large exit slit and the primary monochromator is tuned in steps of typically 50−100 meV (400−800 cm^{-1}). The FEX spectra are corrected for the grating transmission function of the primary monochromator and for the VUV photon flux, respectively. Their spectral resolution is about 30 meV. We show unsmoothed fluorescence spectra in all figures (except Figure 5c), but appropriate smoothed spectra (not shown) were used sometimes to measure the peak locations. A high-resolution VUV absorption spectrum of acetone was used for calibration of the observed FEX spectral wavelengths.

The optimum energy resolution of our photoabsorption spectra[8] (photoelectron spectra[9]) is 3 meV (16 meV), while the absolute precision of the their energy scales is 10 meV (2−3 meV). We note that our measured photoabsorption cross sections are about 15% smaller than those measured by Tabayashi et al.,[4] but this is not surprising in view of the error limit, which is of the same order of magnitude in their work and in our own work.[8] At BESSY I, we measured the quantum yield of ionization, $\gamma(E_{exc})$, between 10 and 19 eV at a resolution of 25−50 meV using a technique previously described.[11] A low-resolution spectrum of γ was measured up to 23 eV at LURE.

Commercial formic acid of highest available purity was used without further purification. We note that eventual contamination with water can easily be revealed during the experiments by observing the well-known fluorescence excitation spectrum of OH ($A^2\Sigma^+ \rightarrow X^2\Pi$) emission, which is known to follow VUV photoexcitation of H_2O between 140 and 100 nm.[12]

3. Results and Discussion

3.1. Energetics of UV and VUV HCOOH Fragmentation Reactions. The existing photophysical data of HCOOH in the energy region under study is summarized in Table 1. This survey of HCOOH electronic states and dissociation channels, the latter shown together with their respective thermochemical threshold energies, will be used in the analysis of the dispersed fluorescence, the FEX spectra, and the total photoion yield (γ) curve.

The lowest-lying excited electronic state $1^1A''$, the photoabsorption cross section to which is very small, has been attributed to the $\pi^* \leftarrow n_o$ transition. The photodissociation dynamics of this state have been studied in detail using laser-induced fluorescence spectroscopy.[13−15] Its origin is experimentally found at 4.64 eV (0_0^0, 37 431 cm^{-1}, 267.2 nm).[13] Nonradiative decay to the ground state with subsequent decomposition into H_2O and CO occurs following excitation close to the origin, whereas at higher excitation energies (>4.94 eV), this state predissociates predominantly into OH and HCO.[14,15]

In the VUV regime, below the first ionization energy (IE, 11.3246 eV), additional valence transitions, as well as many Rydberg series, converging to the first IE, have been identified in the absorption spectrum of HCOOH (see Figure 3).[2,8,16−18] Their absorption cross sections are large as compared to the UV absorption populating the $1^1A''$ state. Above the first ionization energy, we observe increasing photoabsorption until a plateau of about 45 MB is reached at about 18 eV (see Figure 5a). Additional series of Rydberg bands are observed in the 11.3−22 eV absorption region. They are superimposed on a continuous absorption background. These bands, which have been analyzed recently,[8] converge to higher ionization limits the energies of which correspond to the six electronic states of the $HCOOH^+$ ion identified in the He(I) photoelectron spectrum of formic acid.[9,19] The VUV photofragmentation behavior will be discussed in sections 3.2−3.5.

3.2. Dispersed Fluorescence Spectra at Excitation Energy E_{exc} = 12 eV. Figure 1 shows dispersed fluorescence spectra of formic acid at an excitation energy of $E_{exc} = 12$ eV (spectral resolution ≈ 5 nm). The intensity is scaled linearly. We show the unsmoothed original spectrum (Figure 1b), as well as the same unsmoothed spectrum corrected for the response function of the detection system (Figure 1a). The amplitude of the OH ($A^2\Sigma^+ \rightarrow X^2\Pi$) (0−0) band at $\lambda = 308$ nm was used to normalize the intensities of the two spectra with respect to each other. At this excitation energy, we observe two band systems, the first being the OH ($A^2\Sigma^+ \rightarrow X^2\Pi$) emissions at 308 (0−0) and 282 nm (1−0) and the second consisting of a long vibrational progression between 330 and 480 nm (Table 2), the intensity maximum of which is at 375 nm, superimposed on a broad continuous background. These two systems have been observed previously upon VUV excitation of HCOOH at lower excitation energies (6.2−10 eV).[3,20]

3.2.1. OH ($A^2\Sigma^+ \rightarrow X^2\Pi$) Emission. The profiles of the (0,0) and (1,0) bands of OH have been theoretically simulated by

TABLE 1: Energetics of Electronic Transitions and Dissociation Channels of HCOOH and $HCOOH^+$

state/MO transition	band or state energy [eV]	dissociation channels	thermochemical threshold energy [eV]
neutral ground state $1^1A'$	0	neutral dissociation channels	
$1^1A'' \pi^* \leftarrow n_o$ [a]	4.641[b] (origin)	HCO + OH	4.795[c]
		HCOO (X) + H	4.83[d]; 4.85[e]
		HCOO (A) + H	5.366[d]
		COOH + H	4.17[f]
$2^1A'' \pi^* \leftarrow \sigma_{co}$ [a]	broad, E_{max} 7.53 [a]		
$2^1A' \pi^* \leftarrow \pi_{c=o}$ [a]	8−8.8[a]		
Rydberg and valence transitions[a]	8.75−11.5[a]	HCO + OH (A)	8.847[c,g]
		HCOO* + H	9.075[h]
cation ground state $1^2A'$	11.3246[h]	ionic dissociation channels	
		$HCOO^+$ + H	not known[i]
cation excited states		$COOH^+$ + H	12.36[f]
$1\ ^2A''$	12.3783[h]		
		HCO^+ + OH	12.79[j]
		COH^+ + OH	14.21[c]
$2\ ^2A'$	14.81 (IE_v)[h]		
$2\ ^2A''$	15.75 (IE_v)[h]		
$3\ ^2A'$	16.971[h]	HCO^+ + OH (A)	16.84[j,g]
		COH^+ + OH (A)	18.26[c]
		HCO + OH^+(X)	17.97[j]
superexcited molecular states[a]		higher-energy neutral dissociation channels	
		CH (X) + O + OH (X)	13.07[k]
		CH (A) + O + OH (X)	15.95[g,k]
		CH (B) + O + OH (X)	16.3[g,k]
		COOH + H ($n = 4$)	16.92[f]
		COOH + H ($n = 5$)	17.23[f]
		CH (X) + O + OH (A)	17.122[g,k]
		HCOO (X) + H ($n = 4$)	17.58[d]; 17.6[e]
		HCOO (X) + H ($n = 5$)	17.88[d]; 17.9[e]
		HCOO ($^2A_2$) + H ($n = 4$)	18.11[d]
		HCOO ($^2A_2$) + H ($n = 5$)	18.42[d]
		CH (A) + O + OH (A)	20.00[g,k]

[a] See assignments and discussion in ref 8. [b] Reference 13. [c] Reference 31. [d] Reference 24. [e] Reference 21. [f] Reference 45. [g] Reference 32. [h] From the He(I) PE spectrum[9] (see also Figure 5a). [i] The $HCOO^+$ ion is not stable and has so far not been observed experimentally. [j] Reference 46. [k] Reference 47.

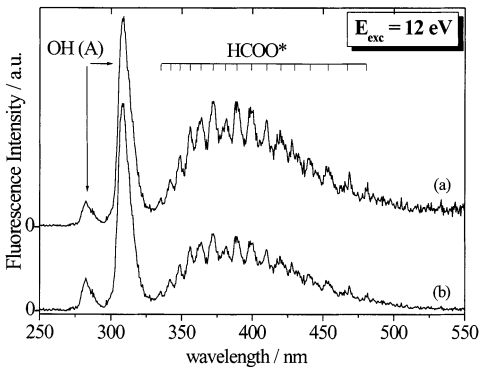

Figure 1. Dispersed fluorescence spectrum observed upon photoexcitation of formic acid at $E_{exc} = 12$ eV (103.3 nm): (a) spectrum corrected for the response function of the fluorescence detection system; (b) uncorrected spectrum. Spectral resolution is ~5 nm. Vertical bars indicate bands listed in Table 2.

TABLE 2: Bands Observed in the Dispersed Fluorescence Spectrum with Formic Acid Excitation Energy $E_{exc} = 12$ eV

wavelength (nm)	energy (cm^{-1})	band spacing (cm^{-1})	corrected intensity (au)
OH ($A^2\Sigma^+ \rightarrow X^2\Pi$) Emission			
308.5 (0−0)	32 415		2500
282.5 (1−0)	35 398		340
HCOO* Emission			
335.3	29 820		330
342	29 240	584	548
348.6	28 690	554	823
355.8	28 110	581	1154
363.4	27 520	588	1255
372	26 880	636	1471
380.7	26 270	614	1243
388.9	25 710	554	1442
399.2	25 050	664	1388
410.1	24 380	666	1215
419.9	23 820	569	1071
429.8	23 270	549	914
440.7	22 690	576	801
453.4	22 060	636	686
467	21 410	642	537
480.4	20 820	597	443

Tabayashi et al.,[4] assuming a thermal Boltzmann population of the $A^2\Sigma^+$ state rovibronic levels, for comparison with the OH fluorescence produced by two-photon (KrF) laser excitation of HCOOH at 9.98 eV (2 × 248.5 nm) and by one-photon (synchrotron radiation) excitation at 9.96 eV and at 11.27 eV. These authors derived OH rotational and vibrational temperatures of the $A^2\Sigma^+$ state as a function of the available excess energy. In our case, we were unable to fit a simulated thermal Boltzmann population of OH $A^2\Sigma^+$ levels to our two observed bands at $E_{exc} = 12$ eV. This is not surprising because there can build up a non-Boltzmann distribution in the $A^2\Sigma^+$ state upon photodissociation of HCOOH at high excess energies (3.153 eV in our case). We also note that the excitation energies in the work of Tabayashi et al.[4] correspond, according to our analysis of the absorption spectrum,[8] to Rydberg excitation of a 10a′ electron, which is mainly nonbonding n_o on the oxygen

atom lone pair of the carbonyl group in HCOOH, whereas in our case, at $E_{exc} = 12$ eV, it is a $\pi_{C=O}$ 2a″ electron that is promoted. The bonding properties are therefore different in these two cases, so the photodissociation dynamics could differ and lead to different energy level population distributions in the OH products.

3.2.2. HCOO Emission and Its Assignment. The work of Dyne, Style, and Ward,[20] using deuterium isotope diagnostics, showed that the emitter of the fluorescence bands between 350 and 450 nm, which they observed upon VUV photon or high-frequency discharge excitation of HCOOH, is most probably the formyloxyl radical, HCOO, in which the hydrogen atom is connected to the carbon atom, and not its isomer, the hydrocarboxy radical COOH (also referred to as HOCO in the literature), which is thermodynamically more stable.[21]

The emitting state of HCOO formed in the VUV dissociation of HCOOH has not been identified hitherto, and one of the objectives of our present work is to assign it. In earlier matrix work on the reaction between fluorine atoms and formic acid, Jacox was able to trap the *t*-HOCO radical in an Ar matrix and assign its infrared absorption spectrum.[22] The isomer HCOO, however, was apparently not stable enough to be trapped and characterized, although there was indirect evidence for its formation.[22]

Lee and Pimentel,[23] upon warming up matrix-isolated CH_2N_2/O_2/Ar mixtures that had been photolyzed at 8 K, observed two chemiluminescence progressions of bands in the same spectral region as our HCOO emission in the gas phase. A set of four bands between 310 and 360 nm were tentatively assigned to the $\tilde{a}^3A'' \rightarrow \tilde{X}^1A'$ transition of formic acid, the latter being formed by reaction of CH_2 ($^3B_1$) with O_2 ($^3\Sigma_g^-$) in the cryogenic matrix, and another set of bands, between 390 and 490 nm, were attributed to the HCOOH $\tilde{A}'^1A' \rightarrow \tilde{A}^1A''$ transition. These two transitions are, respectively, $1^3A'' \rightarrow 1^1A'$ and $2^1A' \rightarrow 1^1A''$ in our nomenclature.[8] The results of Lee and Pimentel might therefore imply that HCOOH, and not HCOO, is the emitter of the VUV excited fluorescence that we observed between 330 and 480 nm in our experiments. We therefore decided to investigate this in more detail, first of all by reconsideration of the experimental findings of Lee and Pimentel.

These authors observed vibrational spacings of about 1390 and 1124 cm^{-1} in the respective assigned $1^3A'' \rightarrow 1^1A'$ and $2^1A' \rightarrow 1^1A''$ transitions of HCOOH. We remark that the 1390 cm^{-1} frequency is greater than, but compatible with, the $\nu_4 =$ 1356 cm^{-1} value calculated for the $1^3A''$ state of HCOOH,[13] of which the $1^3A'' \rightarrow 1^1A'$ O^o_o transition is calculated to be at 3.093 eV, that is, at ∼401 nm, close to the observed 360−390 nm progression, but there are no independent measurements of the energy of the lowest triplet state of formic acid. Observed vibrational frequencies in the $2^1A'$ state are in the 1300−1500 cm^{-1} region,[8] but the $1^1A''$ state has a frequency of 1115 cm^{-1},[13] compatible with the observed 1124 cm^{-1} vibrational spacing. The experimentally determined energy difference between the $2^1A'$ and $1^1A''$ states[8] would give a value 3.467 eV (∼358 nm) for the O^o_o transition which, being greater than that of the observed 390−490 nm progression, is compatible with the displaced oscillators corresponding to the two electronic states involved in the extensive progression.

Because there remained ambiguities concerning the assignment to HCOOH of the two progressions observed by Lee and Pimentel, we decided to directly compare our gas-phase HCOO emission spectra with the chemiluminescence spectra of Lee and Pimentel,[23] taking into account matrix effects. Our study showed that the set of four bands in the 310−360 nm region of Lee and Pimentel can be fitted with four bands in our HCOO spectrum, but this would necessitate an improbable gas to matrix blue shift on the order of 2000 ± 500 cm^{-1}. Furthermore, no correspondence was observed between the 390−490 nm matrix spectrum and our gas-phase spectrum. We add that the $2^1A'$ state of formic acid can be populated already at $E_{exc} = 8.107$ eV,[8] but we observed an onset excitation energy for the gas phase 330−480 nm emission bands (monitored at 375 nm) greater than 9 eV (see later). We thus conclude that HCOOH is not the emitter of the 330−480 nm band progression in the gas phase.

The vibrational spacing is 600 ± 40 cm^{-1} throughout almost the whole HCOO progression at $E_{exc} = 12$ eV. The observed band energies are listed in Table 2 and are shown as bars in Figure 1. The observed bandwidths (fwhm ≈ 150−200 cm^{-1}) are of the same order of magnitude of, and are presumably limited by, the spectral resolution of our detection system (5 nm). The fairly regular spacing of about 600 cm^{-1} corresponds most probably to excitation of the bending mode of the OCO group in the emitter molecule (the corresponding vibrational mode frequency in HCOOH is $\nu_7 = 625$ cm^{-1}),[8,9] and the long progression is indicative of a substantial change in OCO angle in going from the upper to the lower electronic state. The maximum of the HCOO emission is found at about 375 nm in our spectrum. This is at a significantly shorter wavelength than in the observation of Suto et al.[3] at $E_{exc} = 10$ eV, at which the maximum emission wavelength is at about 400 nm. The difference indicates that a significant fraction of the excess energy upon excitation at $E_{exc} = 12$ eV is stored as vibrational energy in the OCO bending mode of excited HCOO.

We remark that Suto et al.[3] did not classify the HCOO emission vibronic bands as a single progression as we have done but into two progressions displaced from each other by 690 cm^{-1}, each of which has an average frequency spacing of 1195 cm^{-1}, unassigned to any specific mode. According to ab initio calculations of Kim et al.,[24] a frequency on the order of 1195 cm^{-1} could correspond to the symmetric CO stretch vibration of HCOO. However, Kim et al. also recorded photoelectron spectra (PES) upon photodetachment of the formate ion, $HCOO^-$. They were thus able to experimentally characterize the three lowest-lying electronic states of HCOO, assuming C_{2v} symmetry, as two quasi-degenerate states, (1^2A_1 as ground state and 1^2B_2, 0.027 eV above) and a third state, 1^2A_2, lying 0.536 eV above the ground state. The $HCOO^-$ PE spectra show partially resolved vibrational features in each state, primarily involving progressions in the OCO bending mode ($\nu = 600-700$ cm^{-1}). Because we see a similar band spacing frequency in our fluorescence spectrum (Table 2), this further confirms the identity of HCOO as the emitting fragment molecule in the VUV excited fluorescence of HCOOH. Additional experiments with higher spectral resolution are required for an accurate assignment of the observed vibronic progression. We turn now to identification of the electronic states involved in the HCOO emission.

We first determine the energies of the upper and lower electronic states in the HCOO emission, using the following data. The fluorescence excitation spectrum of this emission, monitored at 375 nm, presented in section 3.4, shows an onset at $E = 9.075 \pm 0.01$ eV. From the dispersed fluorescence spectrum (Figure 1), the highest energy HCOO emission band is observed to be at $\lambda = 335$ nm (3.7 eV), and we assume that this corresponds to a 0−0 Franck−Condon transition. Assuming further that our observed fluorescence onset energy in the FEX spectrum (9.075 eV) corresponds to a potential barrier of the

corresponding dissociation reaction of no greater than some tenths of 1 eV, we can calculate that the energy of the HCOO state populated by the emission is about 5.375 eV (9.075−3.7 eV) above the ground-state energy of HCOOH. Because the thermochemical threshold for HCOO formation in its ground state from HCOOH dissociation is $E = 4.83$ eV (see Table 1), we can further deduce that the final state of the HCOO fluorescence must lie 0.545 eV above the ground state of this radical. This final (excited) state could be the 1^2A_2 state of HCOO (π-character, C_{2v}), which has been experimentally characterized[24] to be situated 0.536 eV above the HCOO ground state, as mentioned above.

Further information on the HCOO emitting and final states can be obtained from the ab initio calculations of Rauk et al.[25] of the energies of HCOO electronic states in both C_{2v} (two equal carbon−oxygen bond lengths) and C_s (unequal carbon−oxygen bond lengths) symmetries. In C_{2v} symmetry, these authors find twin ground states (σ-states, $^2A_1$ and $^2B_2$) almost degenerate in energy and a π-state ($^2A_2$ symmetry, C_{2v}) lying roughly 0.5 eV above the ground state, agreeing well with the experimental findings of Kim et al.[24] In C_s symmetry, they calculate a $^2A''$ π-state to be energetically close to the $^2A_2$ (C_{2v}) excited state of HCOO. These authors also find a $^2B_1$ π-state (C_{2v}), lying approximately 4 eV above the ground state of HCOO. Because their calculations are successful in reproducing the energies of the three states experimentally characterized by Kim et al.,[24] we go one step further and suggest that the $^2B_1$ state could be the emitting state of HCOO in our experiments. If the final state was the C_s symmetry $^2A''$ π-state, one would expect that the symmetry change from C_{2v} ($^2B_1$) to C_s ($^2A''$) would give rise to excitation of the CO asymmetric stretch mode, calculated to have a frequency on the order of 750 cm^{-1} in the $^2A''$ state.[25] Taking into acount experimental and theoretical uncertainties, this value is not inconsistent with the observed strong vibronic excitation of a mode the frequency of which is on the order of 600 cm^{-1}. However, as assumed and discussed above, an apparently more reasonable mode assignment is the OCO bending mode. This implies that there is a notable change in the OCO bond angle in going from the upper to the lower state. However, in a $^2B_1$ (C_{2v}) to $^2A''$ (C_s) transition, this angle is calculated (CASSCF level)[25] to change from 123.3° to 121.3°, which is a relatively small modification. If the radical remained C_{2v} in both states, so that the lower state was $^2A_2$, the calculated OCO angle change would be 123.3° to 121.1°, an equally small modification. We note that earlier MO calculations in C_{2v} symmetry by Peacock et al.[26] predicted that a $^2B_1 \rightarrow {}^2A_2$ transition would give rise to a band at 386 nm with an oscillator strength of 0.174.

This discussion leads us to suggest that the best assignment of the HCOO fluorescence observed following VUV photodissociation of HCOOH is a $^2B_1$ (C_{2v}) to $^2A''$ (C_s) transition involving excitation of the asymmetric CO mode, possibly coupled to the OCO bending mode. Final assignment requires analysis of a high-resolution emission spectrum of HCOO.

3.3. Dispersed Fluorescence Spectra at Excitation Energy $E_{exc} = 20.66$ eV. *3.3.1. CH and H Balmer Emission at Higher Excitation Energies.* The dispersed fluorescence spectrum obtained on excitation of formic acid at $E_{exc} = 20.66$ eV is shown in Figure 2. Spectral resolution is on the order of 8 nm. OH emission is observed, but HCOO emission is not observed. There are also observed some bands in the 330−500 nm region that were not present at $E_{exc} = 12$ eV. These new bands were assigned by considering their respective excitation spectra, which

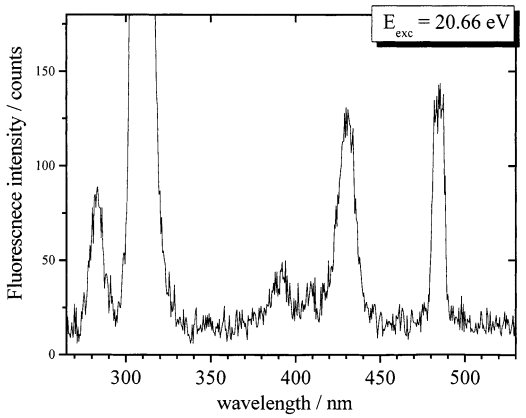

Figure 2. Dispersed fluorescence spectrum observed upon photoexcitation of formic acid at $E_{exc} = 20.66$ eV (60 nm). Spectral resolution is ~8 nm.

are presented in section 3.4, together with the thermochemistry of the related fragmentation processes (Table 1).

The emission band at $\lambda = 431$ nm is broad, so it is necessary to investigate whether it has more than one component. A possible component would be H Balmer-γ ($n = 5 \rightarrow 2$) emission at $\lambda = 434$ nm; another could be the 431.4 nm (0,0) band of the $A^2\Delta \rightarrow X^2\Pi$ transition of the CH radical. H Balmer-γ could result from the dissociation processes HCOOH → COOH + H ($n = 5$) or HCOOH → HCOO + H ($n = 5$), which have thermodynamic onset energies of 17.23 and 17.88 eV, respectively (Table 1). However, these thermodynamic values are higher than the observed onset energy for $\lambda = 431$ nm, which is $E = 16.25 \pm 0.1$ eV, as discussed in section 3.4.3. The value $E = 16.25 \pm 0.1$ eV is consistent with the 15.95 eV thermodynamic threshold of the reaction HCOOH → CH (A) + O + OH (X) (Table 1). We therefore assign the $\lambda = 431$ nm band to CH (A) emission but do not exclude a contribution of H Balmer-γ (5−2) at excitation energies above 17.2 eV (Table 1), especially because the H Balmer-α (3−2) and H Balmer-δ (6−2) emissions were observed at $E_{exc} = 20$ eV (see below).

We next discuss the fluorescence band at $\lambda = 484$ nm, the small bandwidth of which suggests that it is due to an atomic emitter. The wavelength of H Balmer-β emission is 486.1 nm, so at our spectral resolution, this could be the assignment. However, the lowest thermodynamic threshold energy for the appearance of the H Balmer-β emission is 16.92 eV (Table 1), whereas the observed onset energy of $\lambda = 484$ nm is 16.25 ± 0.1 eV (section 3.4.3, Figure 5c), so this atomic emission cannot be present at 16.25 eV. Another possible assignment is to the (0,1) band of the $A^2\Delta \rightarrow X^2\Pi$ transition of the CH radical the Q head of which should occur at 489 nm.

We therefore propose that the 484 nm band is, at least in part, due to the CH $A^2\Delta \rightarrow X^2\Pi$ (0,1) transition. In the fluorescence excitation spectrum of the 484 nm emission, there is a sudden increase in its intensity above 17.6 eV (section 3.4.3, Figure 5c). This is consistent with a H Balmer-β component occurring above 17.6 eV because the opening of the dissociation channel HCOOH → HCOO + H ($n = 4$) has a thermodynamic onset energy that is precisely 17.6 eV (Table 1). Remarkably, as is the case for excitation in the 9−13 eV energy regime, it seems that it is the less-stable isomer HCOO that is preferably formed also at higher excitation energies.

We turn now to a weak emission feature at $\lambda = 410$ nm (Figure 2). This is undoubtedly the H Balmer-δ ($n = 6 \rightarrow 2$) emission line, of which the known wavelength is 410.1 nm. Interestingly, Ma et al.[28] also observe, but do not mention, this

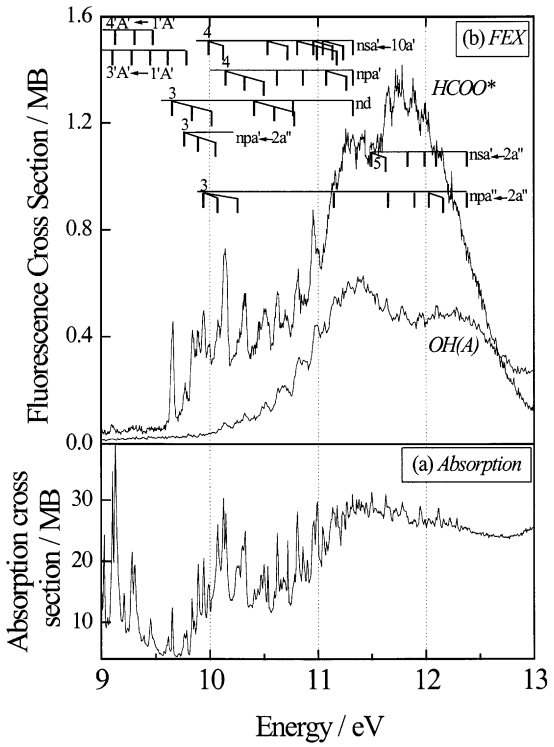

Figure 3. (a) Photoabsorption spectrum of formic acid in the 9−13 eV region[8] and (b) fluorescence excitation (FEX) spectra of formic acid in the 9−13 eV photon excitation region: OH (A) (λ_{obs} = 310 nm) and HCOO* (λ_{obs} = 375 nm) emissions. Vertical bars indicate absorption band assignments.

band upon photoexcitation of CH_3OH at E_{exc} = 27.13 eV (45.7 nm), as well as that of CH_4 at E_{exc} = 22.5 eV (55.1 nm). In additional dispersed fluorescence experiments at LURE, at E_{exc} = 20 eV and with appropriate wavelength detection range, we also observed the H Balmer-α ($n = 3 \rightarrow 2$) emission line at 656.2 nm.

The dispersed fluorescence spectrum also contains a weaker band at λ = 390 nm, which we assign to CH ($B^2\Sigma^- \rightarrow X^2\Pi$) (0,0) band emission. The CH (A−X) and (B−X) bands, which are usually observed in the heads of comets,[27] are also observed, with very similar B/A emission intensity ratios, in the dispersed fluorescence spectrum recorded upon VUV photoexcitation of CH_4 at E_{exc} = 14.87, 16.21, and 22.5 eV and of CH_3OH at E_{exc} = 13.43, 14.87, 16.21, and 27.13 eV.[28] The striking similarity of the B/A emission intensity ratios in all of these spectra suggests that the CH (B) state is populated first and subsequently decays to the A state. In this respect, it is noteworthy that we observe 16.25 ± 0.1 eV as threshold energy for both the (0,0) and (0,1) bands of the $A^2\Delta \rightarrow X^2\Pi$ transition of the CH radical, which is close to the 16.3 eV thermodynamic onset energy for formation of CH ($B^2\Sigma^-$) (Table 1).

It is not at all clear how excited CH is formed in the case of formic acid. The dissociation reaction HCOOH → CH (A,B) + O + OH (X) might be thought to involve as a first step the reaction HCOOH → HCO* + OH (X) in which the formyl radical is formed in a predissociative state. However, it is known that HCO* predissociates into H + CO, not CH and O.[29] Another possible intermediate is HCOH*, because the equivalent ionic reaction $HCOOH^+ \rightarrow HCOH^+ + O$ is known.[5] However, HCOH*, as formaldehyde H_2CO*, predissociates to HCO + H[16,30] and not to CH and OH. Processes such as HCOOH → CH (A,B) + HO_2 or the triple product reaction HCOOH → CH (A,B) + O + OH (X) are unlikely at first glance but must be further explored. Another avenue to explore is excited HCOO as intermediate, in which a large amplitude OCO bending mode vibration could lead to ejection of the CH radical by the process HCOO → CH + O_2.

3.4. Fluorescence Excitation Spectra. In Figure 3, we show the fluorescence excitation (FEX) spectra of the OH $A^2\Sigma^+ \rightarrow X^2\Pi$ (0,0) emission (λ_{obs} = 310 nm) and of the HCOO emission at 375 nm from 9 to 13 eV excitation energy (Figure 3b). For comparison, we also show the photoabsorption spectrum of formic acid (Figure 3a) taken from Leach et al.[8] In this energy region, our measured relative intensity of the OH and HCOO FEX bands is normalized using the absolute fluorescence cross sections given by Tabayashi et al.[4] for photon excitation energies below 11.4 eV. We calculate that at E_{exc} = 12 eV the quantum yield of fluorescence is 1.8% for the OH (A) emission and 4.6% for the HCOO emission. Although our experiments do not allow us to observe neutral fragments in their electronic ground states, on energy grounds (Table 1) it is reasonable to assume that the direct dissociations HCOOH → HCOO (X) + H and HCOOH → HCO + OH (X) are also efficient relaxation pathways of excited states of HCOOH between 6 and 13 eV. This remains to be verified.

We list the observed FEX bands in Table 3, together with the corresponding absorption bands and their transition assignments. We did not attempt to measure the FEX spectra of the 410 and 390 nm emission bands because of their weak intensity. Our analysis of the observed FEX bands is divided into three energy regions: (1) below the first IE (11.3246 eV) (section 3.4.1), (2) from the first IE up to 13 eV (section 3.4.2), and (3) between 13 and 23 eV (section 3.4.3).

3.4.1. Fluorescence Excitation Spectra from 9 eV up to the First IE at 11.33 eV. In this energy region, Rydberg series, converging to the first IE of HCOOH, as well as valence transitions, are found in the absorption spectrum. In Table 3 and Figure 3, we show band assignments according to our recent detailed analysis of the absorption spectrum in the range 6−22 eV.[8]

In the FEX spectra, the weak onset of OH ($A^2\Sigma^+ \rightarrow X^2\Pi$) emission is observed at E_{exc} = 9.15 ± 0.03 eV (136.6 nm), as shown in the threshold region of the OH (A) FEX spectrum in Figure 4. Our measured onset energy value is slightly higher than that reported by Tabayashi et al.[4] (E = 9.05 ± 0.03 eV). From enthalpy of formation (ΔH_f) data[31] and the OH ($A^2\Sigma^+$) T_0 value,[32] we calculate the thermochemical onset for the reaction HCOOH → HCO + OH ($A^2\Sigma^+$) to be 8.85 ± 0.02 eV (Table 1). This is about 300 meV below our measured onset energy of the OH (A) emission. Tabayashi et al.[4] suggest that the difference between the thermochemical and the measured onset energy could indicate the existence of a potential barrier between the HCOOH excited state and the dissociation surface leading to the OH (A) fragment. This is consistent with the slow rise of the OH emission yield in the first electronvolt beyond the onset (Figure 3b), which is typical for photochemical dissociations involving potential barriers. However, we also note that the detection sensitivity for fluorescence photons is limited, so our measured onset energy is, in a sense, an upper limit. This implies that the potential energy barrier for this reaction is probably smaller than the 0.4 eV difference between our measured and the thermochemical onset.

Our observed onset for emission of HCOO is at E_{exc} = 9.075 ± 0.01 eV (136.6 nm) (Figure 3b). Tabayashi et al. report a much lower onset energy (8.16 eV), but this is not evident from their published spectrum.[4] The energetics involved in the formation and relaxation of the HCOO emitting state were discussed in section 3.2.2. In the threshold region, the HCOO

TABLE 3: HCOO* and OH (A) Fluorescence Excitation (FEX) Bands and Corresponding Absorption Bands of HCOOH

HCOO* FEX band position (eV)	HCOO* FEX band position (nm)	OH (A) FEX band position (eV)	OH (A) FEX band position (nm)	nearest HCOOH absorption band (eV)	assignment of the nearest absorption band[8]
9.10	136.25			9.103	$3^1A' \leftarrow 1^1A' (3^1_0)$
9.30	133.3			9.306	$4^1A' \leftarrow 1^1A' (3^2_0)$
9.654	128.43			9.651	$3da' \leftarrow 10a' (0^0_0)$
9.771	126.89			9.763	$3pa' \leftarrow 2a'' (0^0_0)$
				9.782	$3^1A' \leftarrow 1^1A' (3^5_0)$
9.842	125.98			9.835	$3da' \leftarrow 10a' (3^1_0)$
9.891	125.35			9.891	$3pa' \leftarrow 2a'' (6^1_0)$
9.941	124.72			9.942	$3pa'' \leftarrow 2a'' (0^0_0)$
9.992	124.08			9.987	$4sa' \leftarrow 10a' (0^0_0)$
10.08	123.0			10.071	$3pa'' \leftarrow 2a'' (6^1_0)$
10.14	122.27	10.14	122.27	10.125	$4sa' \leftarrow 10a' (6^1_0)$
				10.147	$4pa' \leftarrow 10a' (0^0_0)$
10.271	120.71	10.25	120.96	10.256	$3pa'' \leftarrow 2a'' (3^1_0)$
10.319	120.15	10.325	120.08	10.299	$4pa' \leftarrow 10a' (6^1_0)$
				10.324	$4pa' \leftarrow 10a' (3^1_0)$
10.455	118.59	10.48	118.31	10.442	$4pa' \leftarrow 10a' (6^2_0)$
				10.47	$4pa' \leftarrow 10a' (3^1_0\, 6^1_0)$
10.509	117.98	10.52	117.86	10.498	$4pa' \leftarrow 10a' (3^2_0)$
10.536	117.67			10.533	$5sa' \leftarrow 10a' (0^0_0)$
10.624	116.7	10.64	116.53	10.621	$5pa' \leftarrow 10a' (0^0_0)$
10.706	115.81	10.70	115.87	10.717	$5sa' \leftarrow 10a' (3^1_0)$; $3da'' \leftarrow 2a'' (0^0_0)$
10.792	114.89			10.78	$4da' \leftarrow 10a' (3^2_0)$
10.812	114.67	10.825	114.54	10.806	$6sa' \leftarrow 10a' (0^0_0)$; $5pa' \leftarrow 10a' (3^1_0)$
		10.88	113.96	10.86	$6pa' \leftarrow 10a' (0^0_0)$; $4sa' \leftarrow 2a'' (0^0_0)$
10.958	113.15	10.985	112.87	10.956	$7sa' \leftarrow 10a' (0^0_0)$; $5da' \leftarrow 10a' (3^1_0)$; $5pa' \leftarrow 10a' (3^1_0\, 6^1_0)$
10.998	112.73			10.989	$6sa' \leftarrow 10a' (3^1_0)$; $7pa' \leftarrow 10a' (0^0_0)$; $4sa' \leftarrow 2a'' (6^1_0)$
		11.06	112.1	11.045	$8sa' \leftarrow 10a' (0^0_0)$; $6pa' \leftarrow 10a' (3^1_0)$
11.158	111.12	11.16	111.08	11.148	$4pa'' \leftarrow 2a'' (0^0_0)$; $4sa' \leftarrow 2a'' (3^1_0)$
11.269	110.02	11.285	109.87	11.264	$8pa' \leftarrow 10a' (3^1_0)$
11.324	109.49			11.317	$9pa' \leftarrow 10a' (3^1_0)$
11.412	108.64	11.395	108.81	11.417	
11.503	107.78			11.497	$5sa' \leftarrow 2a'' (0^0_0)$
11.649	106.43	11.635	106.56	11.628	$5sa' \leftarrow 2a'' (6^1_0)$
				11.65	$5pa'' \leftarrow 2a'' (0^0_0)$
11.75	105.52				*a*
		11.78	105.25	11.781	$5pa'' \leftarrow 2a'' (6^1_0)$; $5sa' \leftarrow 2a'' (3^1_0)$
11.884	104.33			11.893	$6pa'' \leftarrow 2a'' (0^0_0)$
		11.95	103.75	11.946	$5pa'' \leftarrow 2a'' (3^1_0)$
11.989	103.42			11.988	$7sa' \leftarrow 2a'' (0^0_0)$
		12.1	102.47	12.116	$7sa' \leftarrow 2a'' (6^1_0)$; $6sa' \leftarrow 2a'' (3^1_0)$
12.14	102.13			12.159	$7pa'' \leftarrow 2a'' (6^1_0)$
12.27	101.05	12.275	101	12.221	$8sa' \leftarrow 2a'' (6^1_0)$
				12.286	$7sa' \leftarrow 2a'' (3^1_0)$
12.49	99.27			*b*	
		13.3	93.2	13.48[c]	$x \leftarrow 9a'$ [c]
		14.2	87.3	14.3	strong continuum
		18.4	67.4	17.9[d]	$x \leftarrow 6a'$ [d]

[a] There is no corresponding absorption feature. [b] Not resolved. [c] Region of broad overlapping Rydberg bands converging to the $2^2A'$ ion state. x = ns, np, and nd Rydberg states. [d] Region of broad overlapping Rydberg bands converging to the $5^2A'$ ion state. x = ns, np, and nd Rydberg states.

FEX spectrum shows a weak band at 9.1 eV, which corresponds to the absorption band that is the first member of a CO stretch vibrational progression of the $\pi^* \leftarrow \pi_1$ ($3^1A' \leftarrow 1^1A'$) transition (Table 3).[8] The first intense band of the HCOO FEX spectrum appears at $E_{exc} = 9.654$ eV, corresponding to the origin band of the $3da' \leftarrow 10a'$ Rydberg transition, and it marks the beginning of a series of sharp bands, which can all be easily associated with features observed in the photoabsorption spectrum (see Table 3 for details). This is also the case for the OH (A) FEX spectrum, which is somewhat less well resolved than the HCOO FEX spectrum because of the weaker intensity of the OH emission. Common to both spectra is that the fluorescence cross section of each of these two emitters increases with increasing photon energy below the first IE. Furthermore, within the limits of their spectral resolutions, it appears that most of the features observed in the OH (A) FEX spectrum are also observed in the HCOO FEX spectrum but with different relative intensities. This is particularly evident, for example, in the energy region between 10 and 11 eV (Figure 3b). It indicates that the corresponding HCOOH excited states can fragment into each of the two dissociation channels. However, as indicated by the different relative intensities of the OH and HCOO FEX bands, the branching ratio of the two dissociation reactions HCOOH → HCO + OH (A) and HCOOH → HCOO ($^2B_1$) + H varies considerably as a function of excitation energy.

3.4.2. Fluorescence Excitation Spectra from the First IE at 11.33 eV up to 13 eV. At energies higher than the first IE, the two FEX spectra in Figure 3b exhibit more marked differences in their evolution. The OH (A) emission intensity decreases with increasing photon energy above the first IE, after reaching a

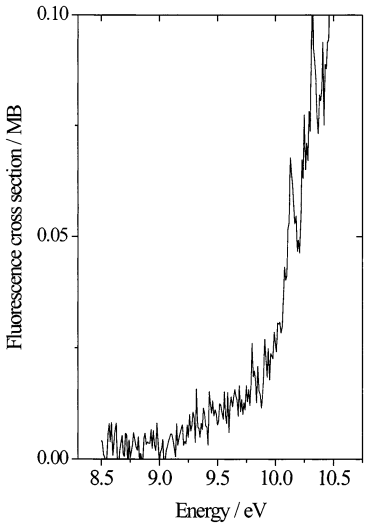

Figure 4. OH (A → X) fluorescence excitation spectrum in the threshold region.

maximum at $E_{exc} = 11.395$ eV, whereas the HCOO emission intensity continues to increase until a maximum is reached at an excitation energy of about $E_{exc} = 11.75$ eV. The OH emission maximum also corresponds to a maximum observed in the photoabsorption curve of HCOOH (Figure 3a).

We note that in this energy region not every OH (A) FEX band can be found in the FEX spectrum of HCOO. The OH (A) FEX bands at $E_{exc} = 11.78$, 11.95, and 12.1 eV are clearly found in the absorption spectrum, corresponding to Rydberg transitions involving promotion of a 2a″ electron (Table 3), but it is difficult to disentangle these bands in the FEX spectrum of HCOO (see Figure 3 and Table 3). Beyond 12 eV, the two FEX spectra differ more markedly. The two signals decrease with increasing photon energy with the HCOO signal falling off rapidly to the background level while the OH (A) fluorescence signal decreases more slowly.

3.4.3. Fluorescence Excitation Spectra between 13 and 23 eV. In Figure 5, we show the FEX spectra of OH (A) emission at higher excitation energies (Figure 5b), as well as the FEX spectra of the emission bands located at $\lambda = 431$ and $\lambda = 484$ nm in the dispersed fluorescence spectrum (Figure 5c). The onsets of the latter have been discussed in section 3.3.1. No HCOO emission was observed at photon energies higher than 13.3 eV. In Figure 5a, we plot the formic acid absorption spectrum, its He(I) photoelectron spectrum, and the quantum yield of ionization, $\gamma(E_{exc})$ as a function of excitation energy.

In the absorption spectrum, we observe three broad bands consisting, respectively, of a shoulder at 13.48 eV and maxima at 14.3 and 17.9 eV. The two bands at 13.48 and 14.3 eV have been attributed to broad overlapping Rydberg transitions, together with their vibrational companions,[8] which probably converge to the second excited state $2^2A'$ ($IE_{vert} = 14.81$ eV) of the ion (see Figure 5a). These two absorption bands correspond to broad bands observed in the FEX spectrum of OH (A). This indicates that neutral dissociation is still an important fragmentation process because OH cannot be formed in its lowest excited $A^2\Sigma^+$ state by any ionic dissociation channel in this energy region (Table 1).

On the other hand, the broad OH (A) FEX band with a shoulder at 17.9 eV and its origin at about 16.8 eV probably corresponds to the dissociative photoionization $HCOOH^+ \rightarrow HCO^+ + OH$ (A), the thermodynamical threshold energy of which is at $E = 16.84$ eV (Table 1). Nishimura et al.[5] recorded threshold photoelectron photoion coincidence (TPEPICO) mass

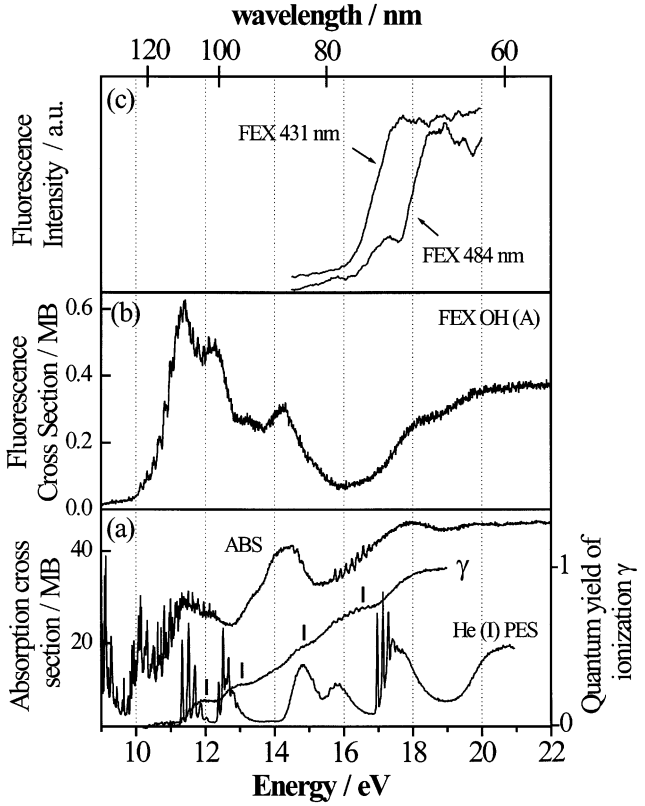

Figure 5. (a) Photoabsorption spectrum,[8] HeI photoelectron spectrum[9] and quantum yield of ionization (γ) of formic acid betwen 9 and 22 eV, (b) fluorescence excitation spectra of OH (A → X) emission, and (c) fluorescence excitation spectra of emission at 431 and 484 nm.

spectra of HCOOH, measuring the ionic fragments as a function of the incident photon energy. They observed a high-energy onset of the formation of the HCO^+ ion at $E \approx 17$ eV, the yield of which reaches its maximum at about 18 eV. This is in excellent agreement with our OH (A) FEX band behavior and thus confirms our suggestion as to its origin. We note that the $HCOOH^+ \rightarrow COH^+ + OH$ (A) dissociation channel, involving formation of the $m/z = 29$ COH^+ isomer in which the hydrogen atom is connected to the O atom, should have a higher appearance energy, which we calculate to be 18.26 eV (Table 1) using the estimated value of its enthalpy of formation given by Lias et al.[31] This may represent an additional channel for formation of OH (A), because Figure 5b shows an increase in the OH (A) emission intensity starting at about 18.3 eV that is mirrored in an increase in the $m/z = 29$ signal at this energy in the breakdown curves given in Figure 2 of Nishimura et al.[5]

In this energy region, we also observe broad bands in the FEX spectrum of the 431 and 484 nm emissions, exhibiting peaks at $E_{exc} = 17.7$ and $E_{exc} = 17.3$ eV, respectively. These emissions have been analyzed in section 3.3.1 and must, on energy grounds, correspond to neutral dissociation. Because the FEX and absorption bands are broad in this energy region, we cannot say whether OH (A) and CH (A) stem from different or common HCOOH superexcited states.

3.5. Photoionization Quantum Yield, γ, and Absorption Spectra in the 9−23 eV Region. *3.5.1. Reaching $\gamma(E_{exc}) = 1$: Autoionization Aspects.* The $\gamma(E_{exc})$ curve grows smoothly with steps occurring whenever an ion state becomes accessible, as discussed in more detail in section 3.5.2. This can be seen when comparing $\gamma(E_{exc})$ with the HeI PE spectrum (Figure 5a, steps are indicated as bars). A similar behavior was found for benzene.[11] This implies that direct ionization of HCOOH is

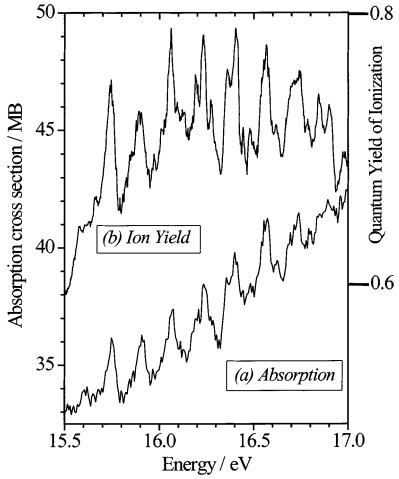

Figure 6. (a) Formic acid absorption spectrum in the 15.5−17 eV region and (b) formic acid ionization quantum yield in the 15.5−17 eV region.

much more important than autoionization of superexcited states. However, HCOOH absorption bands in the 15.7−16.8 eV energy regime, corresponding to Rydberg transitions arising from the 8a′ HCOOH molecular orbital,[8] are clearly seen in the $\gamma(E_{exc})$ curve, indicating autoionization of these states, as discussed below.

Figure 5a shows that the plateau $\gamma(E_{exc}) = 1$ is reached at $E_{exc} = 18 \pm 0.1$ eV. That this plateau extends to at least 23 eV was determined in further ionization quantum yield measurements, carried out at LURE, at a low resolution of ∼200 meV. Defining E_I as the excitation energy value where $\gamma = 1$, we thus determine the energy domain, $\Delta E = E_I - \text{IE}$, of competitive nonionic decay processes of the superexcited molecular states to be 6.68 ± 0.1 eV. This value is similar to that of other astrophysically important small molecules such as CO_2, NH_3, H_2O, and C_2H_4, for which ΔE was found to vary between 6 and 8 eV,[1,33] while for small polycyclic aromatic hydrocarbons (PAHs), $\Delta E \approx 9.2$ eV.[11] Related aspects of the relation between direct ionization and autoionization have been discussed recently by Berkowitz.[34]

It is remarkable that the absorption bands in the 15.7−16.8 eV region appear as features in the ion quantum yield, $\gamma(E_{exc})$, curve, as seen in Figure 5a and in more detail in Figure 6, whereas most of rest of the $\gamma(E_{exc})$ curve is continuous. This behavior indicates that these Rydberg bands, which converge to the $3^2A'$ ion state,[8] undergo autoionization to an ionization continuum on a relatively long time scale. To calculate the autoionization rate, we need to measure the fwhm of the $\gamma(E_{exc})$ and the absorption curve peaks and to compare them, respectively, with the energy resolution of the ion quantum yield and absorption measurements. The $\gamma(E_{exc})$ peaks above the underlying continuum have a fwhm ≈ 50 meV ≈ 400 cm^{-1}. This corresponds to an autoionization rate $k_{ai} \approx 7.5 \times 10^{13}$ s^{-1}, but because the spectral resolution in the $\gamma(E_{exc})$ measurements in the 15.7−16.8 eV region was 50 meV, this k_{ai} value is an upper limit for the autoionization rate. However, the fwhm of the absorption peaks above the underlying continuum in the 15.7−16.8 eV region was also found to have a value of about 50 meV.[8] From this, we infer that the autoionization rate $k_{ai} \approx 7.5 \times 10^{13}$ s^{-1} is a reliable value because the absorption peak fwhm is much greater than the absorption spectral resolution, which is about 10 meV in the 16 eV energy region.[8]

3.5.2. Aspects of Dissociative Ionization. In the following discussion of dissociative ionization in formic acid, we correlate our data on the absorption spectrum, photoelectron spectrum, and ionization quantum yield spectrum with the breakdown curve observations of Nishimura et al.[5] The first step of our γ curve in the region of the first PES band (Figure 5a) corresponds to population of the ion ground state $1^2A'$ (IE = 11.33 eV). This state is stable because no charged fragment is observed below 12 eV.[5] The second step of the γ curve corresponds to the additional population of the first excited state of the HCOOH ion, $1^2A''$ (IE = 12.37 eV).[8,9] This state is not stable because $HCOOH^+$ is no longer observed in the breakdown curves above 12.21 eV and $COOH^+$ appears as the main fragment ion. Steps 3 and 4 of the γ curve can be related to the opening up of population of the ion excited states $2^2A'$ and $2^2A''$, the adiabatic ionization energies of which are ∼14.15 and ∼15.4 eV, respectively.[8,9] Interestingly, the fragmentation behavior of these two ion states is quite similar, as can be deduced from the breakdown diagrams.[5] Both states mainly undergo dissociative photoionization according to $HCOOH^+ \rightarrow COOH^+ + H$ and $HCOOH^+ \rightarrow HCO^+ + OH$, the latter being more important than the former, and it increases considerably in relative yield when the $2^2A''$ state is reached.

The ion state $3^2A'$ ($IE_{ad} = 16.971$ eV),[9] which exhibits a pronounced vibrational structure in the PE spectrum of HCOOH (Figure 5a), also correlates with dissociation into $HCO^+ + OH$ (A) and $COOH^+ + H$. As can be seen from the breakdown curves,[5] the branching ratio of these two reactions varies considerably depending on the exact excitation energy in the 17−18 eV energy region. Measurements of the kinetic energy released in the HCO^+ fragment ion showed that there is a bimodal distribution with a large and a small kinetic energy release (KER) component. The existence of the small KER component led Nishimura et al. to suggest that even at high excitation energies this cation can always be formed in its ground state ($^1\Sigma^+$). Nishimura et al. have therefore questioned whether the dissociation in the 17−18 eV region giving rise to the small KER is a direct process. From the vibrational structure observed in the HeI PES, it is conceivable that the $3^2A'$ state has a relatively long lifetime, so there could exist a fluorescence transition of this ion state to the first excited ion state of $HCOOH^+$ ($1^2A''$), which in turn fragments to produce HCO^+ in its ground state. From the PES spectrum,[9] we estimate that the Franck−Condon maximum of a $3^2A' \rightarrow 1^2A''$ transition would give rise to a fluorescence band at ∼282 nm, which is in the exact spectral region in which we observe the (1,0) band of the OH (A−X) transition. Furthermore, this optical transition should have a small radiative rate because of symmetry selection rules, and a predissociative lower state would create a broad fluorescent band, thus making it even more difficult for us to confirm this suggested pathway for formation of ground-state HCO^+. It is striking, however, that the HCO^+ signal in the PEPICO curves has its onset at 12.6 eV, corresponding to the $HCOOH \rightarrow HCO^+ + OH$ ($X^2\Pi$) channel, which is the energy we estimate to be that of the final state in the Franck−Condon maximum of a $3^2A' \rightarrow 1^2A''$ transition, so there is at present no evidence to negate the proposed fluorescence pathway.

We propose an explanation for another aspect of the observed breakdown curve behavior. In Figure 2b (corrected graph) of Nishimura et al.,[5] the increase in the $COOH^+$ signal begins at about 15.8 eV rising to about 17.3 eV and then drops sharply at higher energies. A similar behavior was also observed by Nishimura et al. for DCOOH in their Figure 3. We propose that the increasing $COOH^+$ signal is produced by dissociative autoionization from the Rydberg levels leading to $3^2A'$ (Figure 6) and decreases when excitation reaches the $4^2A'$ state Franck−

Condon maximum at about 17.3 eV. There is a mirror image behavior for the energy dependence of the formation of HCO^+ (DCO^+), showing that the two channels are competitive if they are formed, as suggested here, by dissociation via autoionization of the Rydberg states. The breakdown curves indicate that the ratio between the $H + COOH^+$ and the $OH + HCO^+$ dissociative autoionization channels increases with increasing energy in the 15.8−17.3 eV region. A study of the breakdown curves of formic acid at an adequately high spectral resolution is necessary to confirm our proposed dissociative autoionization interpretation.

4. Conclusions and Astrophysical Implications

Photofragment fluorescence spectroscopy was used to study the VUV photofragmentation of formic acid in the 6−23 eV energy regime. We also recorded the quantum yield of photoionization (γ) as a function of the incident photon energy. Recent studies of the photoabsorption[8] and the photoelectron spectrum[9] of HCOOH in the same energy region were used to analyze the observations.

When HCOOH is excited with photon energies that correspond to astrophysical HI regions ($E_{photon} < 13.6$ eV), we detect OH ($A^2\Sigma^+ \rightarrow X^2\Pi$) and HCOO emissions in the UV/visible spectral region. Because the ionization energy of HCOOH is 11.33 eV, this indicates that the neutral photoreactions $HCOOH \rightarrow OH\ (A^2\Sigma^+) + HCO$ and $HCOOH \rightarrow HCOO^* + H$ are important photodissociation pathways that must be considered in the gas-phase astrochemistry of this molecule. From the FEX spectra of the two fluorescence signals, we conclude that the branching ratio of the two photoreactions depends on the nature of the initially populated state and its interaction with dissociative neutral states. All features seen in the FEX spectra of OH (A) and HCOO can be associated with absorption bands of HCOOH. Because absolute absorption and fluorescence cross sections are available, it is in principle possible to estimate state-selective quantum yields for the two dissociation channels in the energy range investigated here, but this has not been attempted in the present study. We further conclude from our study that the emitting state of HCOO is most likely 1^2B_1 (C_{2v}) and the lower state $1^2A''$ (C_s), states that were characterized in the ab initio calculations of Rauk et al.[25]

Although, in our experiments, we cannot observe nonfluorescing neutral fragments, it is reasonable to assume that also the photodissociations $HCOOH \rightarrow OH + HCO$ and $HCOOH \rightarrow HCOO + H$, leading to the fragments in their respective electronic ground states, are important. The yields of these two processes, however, remain to be quantified. HCOO is thermodynamically unstable with respect to CO_2 and H by 0.58 eV. It is possible that HCOO, after formation in the excited 1^2B_1 state and radiative relaxation to the $1^2A''$ state, undergoes fragmentation into these neutral products. The photodissociation processes $HCOOH \rightarrow CO_2 + 2H$ (via excited-state relaxation of HCOO) and $HCOOH \rightarrow OH + HCO$ would thus constitute the most efficient fragmentation pathways of formic acid below the astrophysical HI limit.

The dissociative photoionizations $HCOOH^+ \rightarrow COOH^+ + H$ and $HCOOH^+ \rightarrow HCO^+ + OH$ are energetically possible above 12.22 and 12.79 eV, respectively. We can conclude from our measurement of the quantum yield of ionization that the sum of the respective quantum yields of these two ionic channels at energies below the astrophysical HI limit is less than the value at 13.6 eV, at which we measure $\gamma = 0.25$ (Figure 5a). On the other hand, $COOH^+$ is observed in the ISM,[7] where it could be produced, at least in part, from formic acid.

At higher excitation energies ($E_{exc} > 13.6$ eV), OH (A) fluorescence is also detected. Its FEX spectrum shows broad bands that coincide with broad photoabsorption features that have been attributed by Leach et al.[8] to Rydberg series converging to higher ionization limits. Between 13.6 and 16.8 eV, OH (A) is formed by neutral processes, whereas above 16.8 eV, it is most likely formed also by the dissociative photoionization $HCOOH^+ \rightarrow HCO^+ + OH$ (A). Above 16 eV, we detect CH ($A^2\Delta \rightarrow X^2\Pi$) (0,0; 0,1) fluorescence indicating that neutral photodissociation of HCOOH to form CH (A) takes place at these energies through a formation process that remains to be clarified. Above 17.7 eV, there is a rapid increase in the 484 nm signal intensity, which we attribute to a contribution from hydrogen Balmer-β emission indicating that the photodissociation $HCOOH \rightarrow HCOO + H$ ($n = 4$) takes place in this energy region.

The quantum yield of photoionization (γ) of HCOOH exhibits a steplike behavior as a function of the incident photon energy. These steps occur whenever an ion state of HCOOH is accessible, and they also coincide with maxima in the TPEPICO breakdown curves of charged photofragments of HCOOH.[5] Every step in the γ curve can be associated with the opening of a new ionic fragmentation channel. The energy domain ΔE of competitive nonionic decay processes of superexcited molecular states is found to be $\Delta E = 6.68 \pm 0.1$ eV for formic acid. This is similar to the case of small molecules such as CO_2, H_2O, NH_3, and C_2H_4.[1,11,33] One particularly interesting observation in the case of formic acid is that Rydberg absorption bands converging to the $3^2A'$ state of $HCOOH^+$ are mirrored in the $\gamma(E_{exc})$ spectrum between 15.7 and 17 eV. An autoionization rate of $k_{ai} \approx 7.5 \times 10^{13}\ s^{-1}$ was determined for the Rydberg levels. Furthermore, we propose that competitive dissociative autoionization processes from these Rydberg levels are responsible for the increasing $COOH^+$ signal and decreasing HCO^+ signal observed in the breakdown curves of Nishimura et al.[5] above 15.8 eV. The relative signal strengths are modified when excitation reaches the $4^2A'$ state Franck−Condon maximum at about 17.3 eV.

Our results were used to pay particular attention to another aspect of the formic acid ion breakdown curves of Nishimura et al.[5] We discussed the observational implications of their suggestion that there could exist a fluorescence transition of the $3^2A'$ ion state to the first excited ion state of $HCOOH^+$ ($1^2A''$), which in turn fragments to produce HCO^+ in its ground state, and showed the difficulty of its experimental verification.

Our results demonstrate that the spectroscopy and photophysics of formic acid have potential applications in astrophysics and exobiology, in particular, for understanding the formation and dissociation of this species, as well as its dissociation products. Formic acid is one of the potential building blocks of biomolecules[35] and has been observed by radioastronomy in several sites in the interstellar medium (ISM), for example, in the cold dark cloud L134N and in W51, a region of massive star formation.[36] Furthermore, this molecule is found in comets,[37] which are thought to be one of the possible sources of extraterrestrial supply of organic material to the early Earth.[6] HCOOH and the formate ion ($HCOO^-$) have been proposed, among other species, to be the carriers of weak infrared absorption features at 7.24 and 7.41 mm observed in the young stellar object W33A by the short wavelength spectrometer (SWS) on board of ISO Infrared Space Observatory.[38] HCOOH is also observed in high yield in Miller/Urey experiments, which simulate the evolution of early Earth atmospheres.[39] $HOCO^+$, which is protonated CO_2, is also one of the ionic fragments

produced by dissociative ionization of formic acid.[5] It has been observed in the galactic center region and in Sgr B2.[40,41] The photophysical properties of HCOOH are thus of direct interest for radioastronomy searches, as well as for an understanding of observations on comets and interstellar ices containing HCOOH and its dissociation products. Present models of the formation and destruction of these species are inconclusive,[6,38,41−43] and new approaches[44] are worth considering.

Acknowledgment. We thank Jean-Louis Chotin, Christian Alcaraz, Saoud Baouch, and Daniel Tepfer for their valuable assistance during the synchrotron radiation beam time periods, as well as Klaus Hottmann for carefully recording the He(I) photoelectron spectrum of formic acid. M.S. acknowledges the TMR program of the European Union under Contract FMRX-CT97-0126 on "Usable Fullerene Derivatives" (USEFULL) for financial support. H.W.J. is grateful for support from the European Commission program "Access to Research Infrastructures". Welcome support from the CNRS Groupe de Recherche "GDR Exobiologie" and from INSU is gracefully acknowledged.

References and Notes

(1) Berry, R. S.; Leach, S. *Adv. Electron. Electron Phys.* **1981**, *57*, 1.
(2) Robin, M. B. *Higher Excited States of Polyatomic Molecules*; Academic Press: New York, 1974; Vol. 1.
(3) Suto, M.; Wang, X.; Lee, L. C. *J. Phys. Chem.* **1988**, *92*, 3764.
(4) Tabayashi, K.; Ayoama, J.; Matsui, M.; Hino, T.; Saito, K. *J. Chem. Phys.* **1999**, *110*, 9547 and references therein.
(5) Nishimura, T.; Meisels, G. G.; Niwa, Y. *J. Chem. Phys.* **1989**, *91*, 4009.
(6) Chyba, C.; Sagan, C. *Nature* **1992**, *355*, 125.
(7) (a) Herbst, E.; Klemperer, W. *Astrophys. J.* **1973**, *185*, 505. (b) Watson, W. D. *Annu. Rev. Astron. Astrophys.* **1978**, *16*, 585. (c) Herbst, E. *Annu. Rev. Phys. Chem.* **1995**, *46*, 27.
(8) Leach, S.; Schwell, M.; Dulieu, F.; Chotin, J.-L.; Jochims, H.-W.; Baumgärtel, H. *Phys. Chem. Chem. Phys.* **2002**, *4*, 5025.
(9) (a) Schwell, M.; Leach, S.; Hottmann, K.; Jochims, H.-W.; Baumgärtel, H. *Chem. Phys.* **2001**, *272*, 77. (b) Leach, S.; Schwell, M.; Talbi, D.; Berthier, G.; Hottmann, K.; Jochims, H.-W.; Baumgärtel, H. *Chem. Phys.*, in press.
(10) Whitehead, C. *Annu. Rep. R. Soc. Chem., Sect. C* **1999**, *94*, 293.
(11) Jochims, H.-W.; Baumgärtel, H.; Leach, S. *Astron. Astrophys.* **1996**, *314*, 1003.
(12) Lee, L. C.; Suto, M. *Chem. Phys.* **1986**, *110*, 161.
(13) Ioannoni, F.; Moule, D. C.; Clouthier, D. J. *J. Phys. Chem.* **1990**, *94*, 2290.
(14) Brouard, M.; Wang, J.-X. *J. Chem. Soc., Faraday Trans.* **1992**, *88*, 3511.
(15) Brouard, M.; Simons, J. P.; Wang, J.-X. *Faraday Discuss. Chem. Soc.* **1991**, *91*, 63.
(16) Herzberg, G. *Molecular Spectra and Molecular Structure − Vol. III, Electronic Spectra and Electronic Structure of Polyatomic Molecules*; Van Nostrand Reinhold: New York, 1966.
(17) Bell, S.; Ng, T. L.; Walsh, A. D. *J. Chem. Soc., Faraday Trans.* **1974**, *71*, 393.
(18) Fridh, C. *J. Chem. Soc., Faraday Trans.* **1977**, *74*, 190.
(19) Kimura, K.; Katsumata, S.; Yamazaki, T.; Wakabayashi, W. *J. Electron Spectrosc. Relat. Phenom.* **1975**, *6*, 41.
(20) (a) Dyne, P. J.; Style, D. W. G. *J. Chem. Soc.* **1952**, 2122. (b) Style, D. W. G.; Ward, J. C. *J. Chem. Soc.* **1952**, 2125.
(21) Langford, S. R.; Batten, A. D.; Kono, M.; Ashfold, M. N. R. *J. Chem. Soc., Faraday Trans.* **1997**, *93*, 3757.
(22) Jacox, M. *J. Chem. Phys.* **1988**, *88*, 4598.
(23) Lee, Y.-P.; Pimentel, G. C. *J. Chem. Phys.* **1981**, *74*, 4851.
(24) Kim, E. H.; Bradford, S. E.; Arnold, D. W.; Metz, R. B.; Neumark, D. M. *J. Chem. Phys.* **1995**, *103*, 7801.
(25) Rauk, A.; Dak, Y.; Borowzski, P.; Roos, B. *Chem. Phys.* **1995**, *197*, 73.
(26) Peacock, T. E.; Rahman, R.-U.; Sleeman, D. H.; Tuckley, E. S. G. *J. Chem. Soc.* **1963**, 144.
(27) Festou, M. C.; Rickman, H.; West, R. M. *Astron. Astrophys. Rev.* **1993**, *4*, 363; *5*, 37.
(28) Ma, G.; Suto, M.; Lee, L. C. *J. Quant. Spectrosc. Radiat. Transfer* **1990**, *44*, 379.
(29) Loettgers, A.; Untch, A.; Stumpf, M.; Schinke, R.; Werner, H.-J.; Bauer, C.; Rosmus, P. *Chem. Phys. Lett.* **1994**, *230*, 290.
(30) Okabe, H. *Photochemistry of small molecules*; John Wiley: New York, 1978.
(31) Lias, S. G.; Bartmess, J. E.; Liebmann, J. F.; Holmes, J. L.; Levin, R. D.; Mallard, W. G. *J. Phys Chem. Ref. Data* **1988**, *17* (Suppl. 1).
(32) Huber, K. P.; Herzberg, G. Constants of Diatomic Molecules (data prepared by Gallagher, J. W. and Johnson, R. D., III). In *NIST Chemistry WebBook*, Mallard, W. G., Linstrom, P. J., Eds.; NIST Standard Reference Database Number 69; National Institute of Standards and Technology: Gaithersburg, MD, 2000; http://webbook.nist.gov.
(33) Leach, S. In *Polycyclic Aromatic Hydrocarbons and Astrophysics*; Léger, A, d'Hendecourt, L., Boccara, N., Eds.; Reidel: Dordrecht, Netherlands, 1987; p 99 ff.
(34) Berkowitz, J. *Phys. Essays* **2000**, *13*, 248.
(35) Brack, A. *The Molecular Origins of Life*; Cambridge University Press: Cambridge, U.K., 1998.
(36) Irvine, W. M.; Friberg, P.; Kaifu, N.; Matthews, H. E.; Minh, Y. C.; Ohishi, M.; Ishikawa, S. *Astron. Astrophys.* **1990**, *229*, L9.
(37) Cottin, H.; Gazeau, M.-C.; Raulin, F. *Planet. Space Sci.* **1998**, *47*, 1141.
(38) Schutte, W. A.; Boogert, A. C. A.; Tielens, A. G. G. M.; Whittet, D. C. B.; Gerakines, P. A.; Chiar, J. E.; Ehrenfreund, P.; Greenberg, J. M.; de Graauw, Th. *Astron. Astrophys.* **1999**, *343*, 966.
(39) Miller, S. L. In *The Molecular Origins of Life*; Brack, A., Ed.; Cambridge University Press: Cambridge, U.K., 1998; p59.
(40) Thaddeus, P.; Guélin, M.; Linke, R. A. *Astrophys. J.* **1981**, *246*, L41.
(41) Minh, Y. C.; Brewer, M. K.; Irvine, W. M.; Friberg, P.; Johansson, L. E. B. *Astron. Astrophys.* **1991**, *244*, 470.
(42) Bockelée-Morvan, D.; Lis, D. C.; Wink, J. E.; Despois, D.; Crovisier, J.; Bachiller, R.; Benford, D. J.; Biver, N.; Colom, P.; Davies, J. K.; Gérard, E.; Germain, B.; Houde, M.; Mehringer, D.; Moreno, R.; Paubert, G.; Philipps, T. G.; Rauer, H. *Astron. Astrophys.* **2000**, *353*, 1101.
(43) Rodgers, S. D.; Charnley, S. B. *Mon. Not. R. Astron. Soc.* **2001**, *320*, L61.
(44) Chevreau, H.; Boullant, E.; Dézarnaud-Dandine, C.; Sevin, A. *Chem. Phys.* **2000**, *254*, 99.
(45) Rusic, B.; Litorja, M. *Chem. Phys. Lett.* **2000**, *316*, 45.
(46) Warneck, P. *Z. Naturforsch., A* **1974**, *29*, 350.
(47) Chase, M. W., Jr. NIST-JANAF Themochemical Tables, Fourth Edition. *J. Phys. Chem. Ref. Data* **1998**, *Monograph 9*, 1.